ISSN (Print) 1226-1750
ISSN (Online) 2233-6656
Journal of Magnetics 23(4), 680-688 (2018) https://doi.org/10.4283/JMAG.2018.23.4.680

A Study on the Effective Deperming Protocol Considering Hysteresis Characteristics in Ferromagnetic Material

Sang Hyeon Im[1], Ho Yeong Lee[1], Hyun Ju Chung[2], and Gwan Soo Park[1]*

[1]*Department of Electrical and Computer Engineering, Pusan National University, Busan 46241, Republic of Korea*
[2]*Naval Systems R&D Institute, Agency Defense Development, Changwon 51678, Republic of Korea*

(Received 14 July 2018, Received in final form 14 September 2018, Accepted 2 October 2018)

Demagnetization is crucial in national defense and is applied by deperming protocols. However, because a warship has an open structure, it is inevitable that demagnetizing fields are generated and magnetic fields that are different from the intended are applied. Therefore, in this paper, the effect of the demagnetizing field during the demagnetization process was analyzed. The magnetization distribution was simulated using a program combining the finite element method and Preisach model, and verified through experiments using specimens. In addition, experiments using scaled-down warship were performed. From the experimental results, we confirmed that Deperm-ME is superior to Anhysteretic, because the internal applied magnetic field was constantly applied.

Keywords : demagnetization, demagnetizing field, preisach model, anhysteretic, Deperm-ME

1. Introduction

Demagnetization is technique of removing residual magnetization in a magnetic material. It is used in various fields such as HDD and VFD to record and erase data. Particularly, in national defense, it is crucial to prevent the damage caused by magnetic mines. Since a warship is made of a ferromagnetic material, residual magnetization is inevitably generated. To reduce the residual magnetization, magnetic fields that are continuously alternating and decreasing are applied, and these are called the deperming protocol [1-3].

Three types of deperming protocols are currently used globally: Anhysteretic deperm, Deperm-ME, and Flash-D. However, these techniques have been depended on the experiments and experience of advanced countries rather than theory. Further, the advantages and disadvantages of each protocol have not been clearly investigated; therefore, the effective protocol is difficult to choose depending on the situation.

*Corresponding author: Tel: +82-51-510-2788
Fax: +82-51-513-0212, e-mail: gspark@pusan.ac.kr

This paper was presented at the IcAUMS2018, Jeju, Korea, June 3-7, 2018.

Recently, demagnetization has been studied for theoretical analysis [4-8]. To analyze the characteristics of the protocols, it is important to consider the magnetic field applied inside the vessel. In Anhysteretic and Deperm-ME, these fields are simulated using the Preisach model combined with the finite element method (FEM) [9]. However, the analysis on the cause of the applied field in a magnetic material is insufficient, and the corresponding experiment has not been performed.

When magnetic fields are applied from the outside to a ferromagnetic material, demagnetizing fields that are determined by the demagnetizing factor and magnetization are generated inside. The demagnetizing factor is constant because the shape and magnetization become nonlinear depending on the hysteresis characteristic. Consequently, the demagnetizing field occurs nonlinearly and finally the magnetic field applied to the inside is changed.

In this paper, the deperming protocol has been studied to reduce the residual magnetization in consideration of the demagnetizing field. Even if the residual magnetization is reduced, after the departure, it may be exposed to the earth magnetic field, resulting in a large magnetization. In order to prevent this, a reverse magnetize method is also used. However, this study focuses on the method of reducing the residual magnetization. The effect of the demagnetizing field and deperming results were analyzed using the Preisach model. In addition, it was verified

using the SPCC specimen and the SS400 scaled-down warship in a magnetic treatment facility. The results of the theoretical analysis and the experiments show good agreement with each other.

2. Effect of Demagnetizing Field on Demagnetization

A warship made of ferromagnetic materials is magnetized by an external environment and has a residual magnetization. To reduce the residual magnetization, demagnetization is necessary. Hence, alternating and decreasing magnetic fields are applied using coils that are installed on the outside. These fields cause the magnetic material to gradually create a minor curve along with the hysteresis characteristic. The magnetization is gradually reduced, and finally, very little magnetization remains. This process is shown in Fig. 1.

However, since it has an open structure at both ends, demagnetizing fields are generated. Magnetic fields that are different from the external field are applied to the inside, as shown in Fig. 2. Therefore, in this study, the

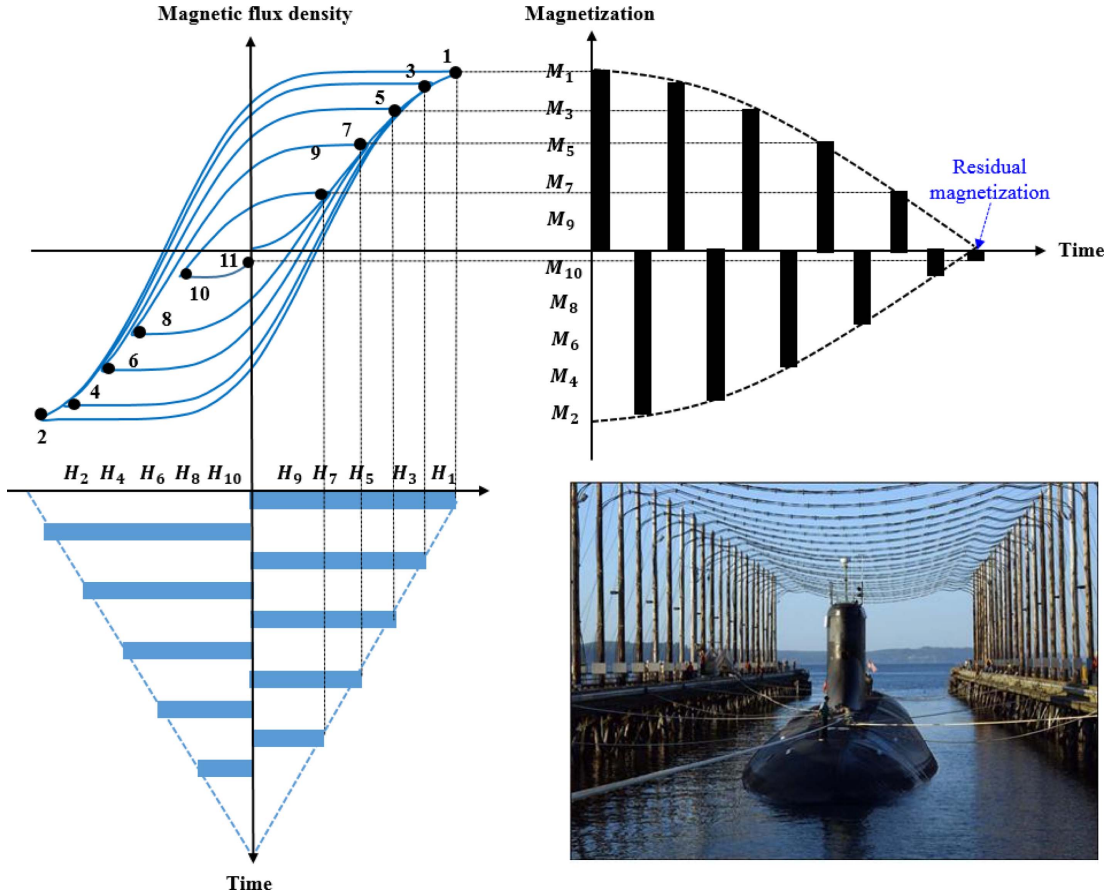

Fig. 1. (Color online) Hysteresis characteristics during demagnetization in the warship model.

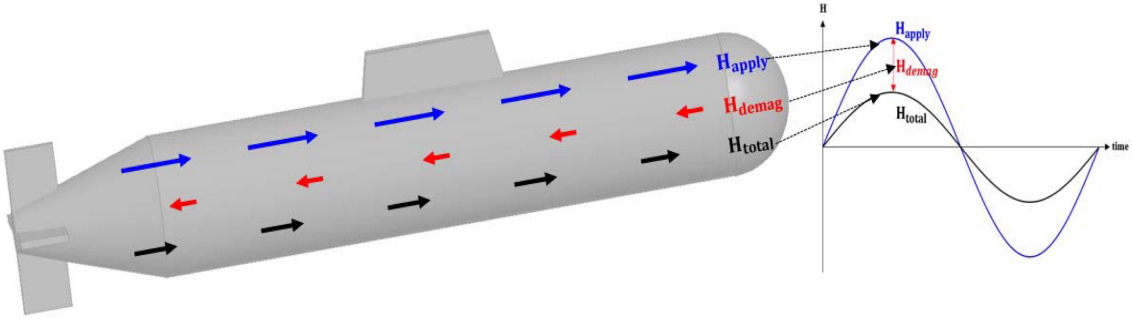

Fig. 2. (Color online) Schematic of magnetic field types and distribution in the warship.

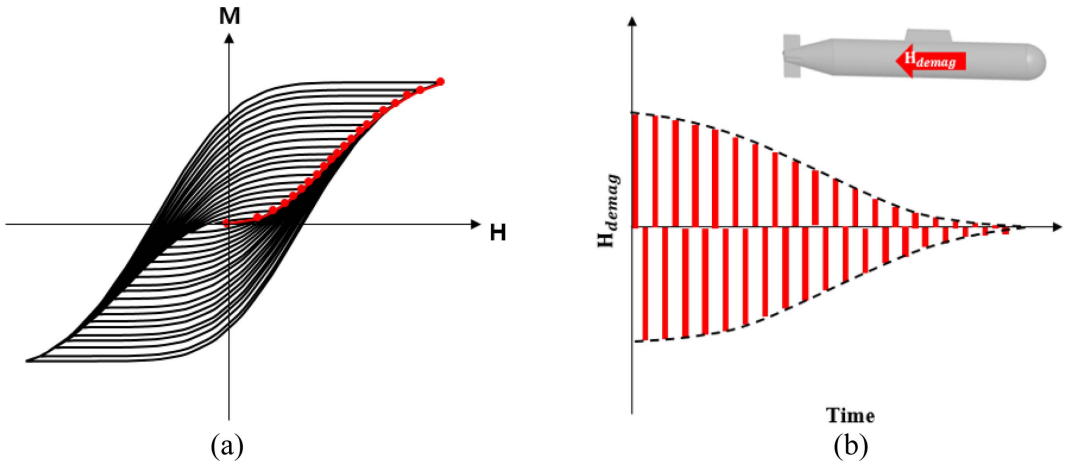

Fig. 3. (Color online) Magnetization curves and demagnetizing fields generated during demagnetization: (a) Magnetization curve by applied magnetic field, (b) Demagnetizing fields.

effect on the demagnetizing field is analyzed.

2.1. Influence of demagnetizing fields during demagnetization process

The demagnetizing field is determined by the demagnetizing factor N_d and magnetization $\vec{M}$ by (1). To analyze the field, two components must be considered. First, the demagnetizing factor is primarily determined by the shape of the object; therefore, it is represented as one value in the model [10-12].

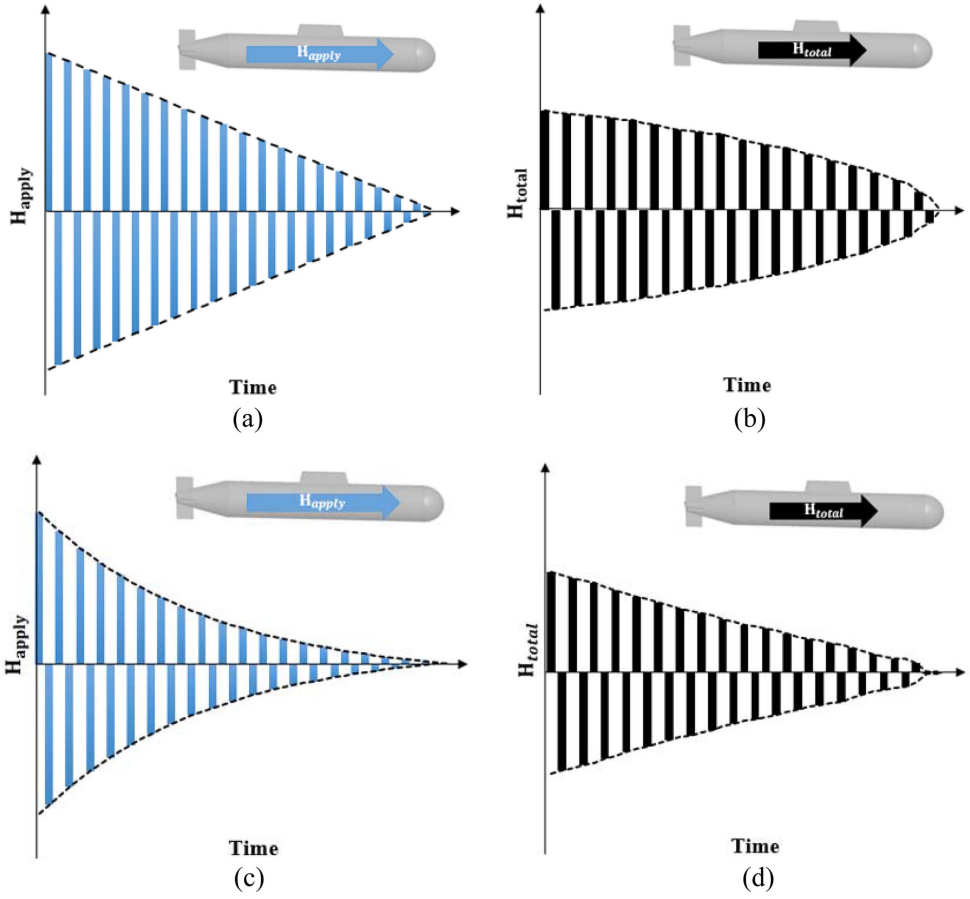

Fig. 4. (Color online) Deperming protocols and total magnetic field depending on the influence of the demagnetizing field: (a) Anhysteretic protocol. (b) Total magnetic field in Anhysteretic. (c) Deperm-ME protocol. (d) Total magnetic field in Deperm-ME.

$$\overrightarrow{H_d} = N_d \overrightarrow{M} \quad (1)$$

However, the magnetization cannot be represented as one value depending on the hysteresis characteristic, and changes according to the applied field. When the deperming protocol was applied, it was determined along the minor curve from the major curve and became nonlinear, as shown in Fig. 3(a). Therefore, during the demagnetization process, it was generated nonlinearly by the demagnetizing factor and magnetization, as shown in Fig. 3(b).

The demagnetizing field reduces the magnetic field applied from the outside. The total magnetic field, $\overrightarrow{H_t}$ that is actually applied inside the object is represented by (2), a subtraction of the demagnetizing field $\overrightarrow{H_d}$ from the externally applied field $\overrightarrow{H_a}$.

$$\overrightarrow{H_t} = \overrightarrow{H_a} - \overrightarrow{H_d} \quad (2)$$

To analyze the effect of the demagnetizing field on demagnetization, we applied it to the Anhysteretic and Deperm-ME protocols that are primarily used. In the linearly decreasing Anhysteretic, the total magnetic field decreases in a bell-shaped form owing to the nonlinear demagnetizing fields, as shown in Fig. 4(b). Consequently, the decrement increases as time progresses during the demagnetization. Meanwhile, if the nonlinearly decreasing Deperm-ME is applied, the internal magnetic field becomes linear, as shown in Fig. 4(d).

2.2. Analysis using the Preisach model

In this study, the Preisach model was used to analyze the effect of the internal magnetic field. In the Preisach model, the hysteresis characteristic of the magnetic material was expressed by Preisach density distribution on the plane of a triangle. Each particles is represented as a unit hysteresis operator with α and β. Since α and β are different depending on the particles, the density of the operators can be expressed as p(α, β) each axis as shown in Fig. 5.

Subsequently, the traces were drawn according to the applied field on the Preisach plane and divided into two regions. Since the decrement became larger in the Anhysteretic protocol, the traces were drawn densely at the low density region, and sparsely at the high density region, as shown in Fig. 6(a). The total magnetization after deperming is determined by integrating the densities of the two regions by (3). Integrating the densities of the two regions divided by the traces, a large magnetization would be generated. That is, the residual magnetization after applying Anhysteretic is large.

$$Magnetization = \iint_{S+} p(\alpha,\beta)d\alpha d\beta - \iint_{S-} p(\alpha,\beta)d\alpha d\beta \quad (3)$$

On the other hand, in the Deperm-ME protocol, the density distribution in the Preisach plane was uniformly divided, as shown in Fig. 6(b), because it has a constant decrement of the total magnetic fields. As a result, the density distribution in the two regions became similar, and if the entire density is integrated, it became very small. Therefore, the magnetization became smaller than the Anhysteretic, and superior demagnetization results were obtained.

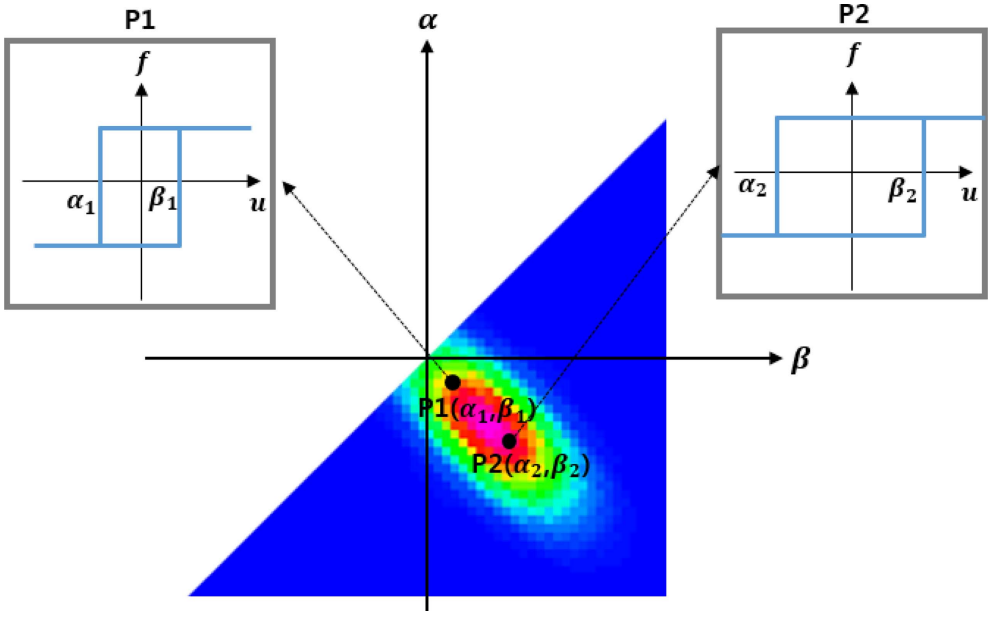

Fig. 5. (Color online) Schematic of Preisach density distribution and unit hysteresis operator on the Preisach plane.

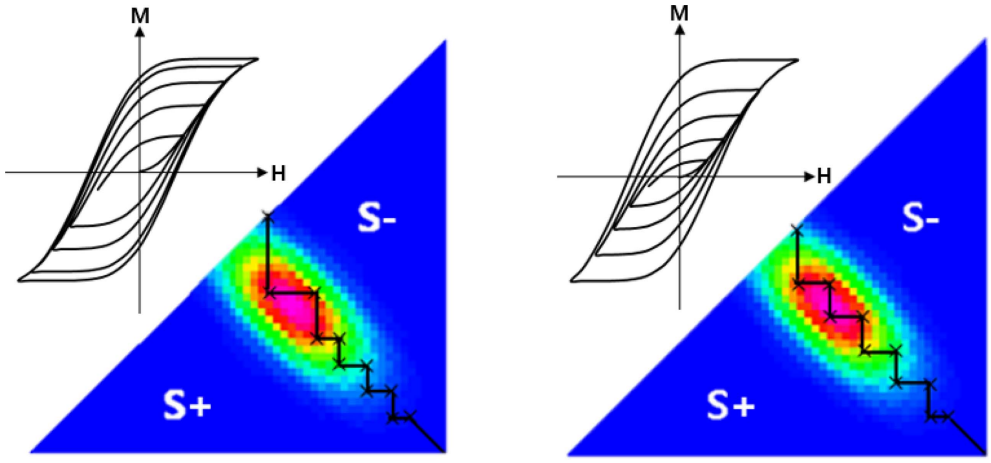

(a) (b)

Fig. 6. (Color online) Traces on the Preisach plane according to two protocols: (a) Anhysteretic. (b) Deperm-ME.

3. Simulated and Experimental Results

To verify the influence of the demagnetizing fields according to the Anhysteretic and Deperm-ME protocol, laboratory-scale experiments using a magnetic treatment facility (MTF) were performed and simulated by the Preisach model combined with the FEM. A hollow cylinder specimen of the SPCC and a scaled-down warship made of SS400 were used. Fig. 7 shows the B–H curves for the two materials. SS400 has a coercive force that is twice as large as that of SPCC, and the similar squareness ratio.

3.1. Simulated and experiment results using SPCC specimen

First, a simulation was conducted using Preisach modeling combined with the FEM. The SPCC material characteristics were represented by the Preisach model and input to the demagnetization object, modeled as shown in Fig. 8(a). A solenoid coil having a length of 565 mm and a diameter of 60.4 mm is modeled and deperming protocols were applied to it. A specimen with a length of 298 mm and an outer diameter of 44 mm and an inner diameter of 42 mm was modeled inside the coil to demagnetize. After demagnetization, magnetic flux density was measure

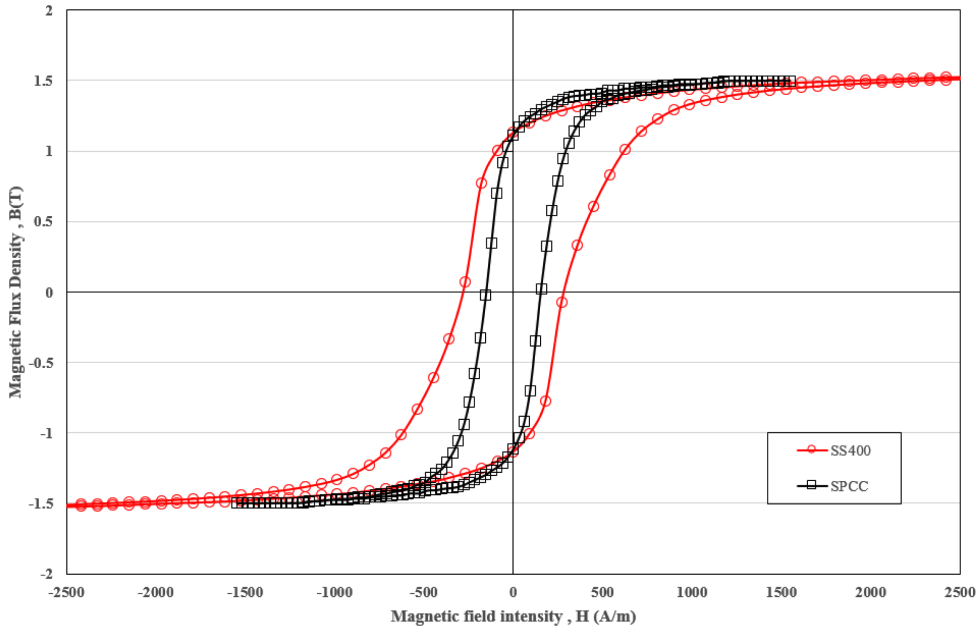

Fig. 7. (Color online) Hysteresis characteristics of SPCC and SS400.

Table 1. Parameters of Anhysteretic and Deperm-ME protocol.

Parameter	Anhysteretic Deperm	Deperm-ME
Shots [Number]	36	36
The first amplitude of magnetic field [A/m]	2000	2000
The last amplitude of magnetic field [A/m]	55.6	131.6
The decrement of magnetic field [A/m]	55.6	$e^{-0.06x}$

under 18 cm below the specimen.

Table 1 shows the parameters of the Anhysteretic and Deperm-ME protocols. The amplitude of the initial magnetic field and the number of shots were the same, and the decrement was applied differently. After applying the two protocols to the deperming coil, the residual magnetization distribution was compared. Fig. 8(b) and (c) show the cross section at the center of specimen after demagnetization. As a result of applying Anhysteretic, very large magnetization remains in the specimen and it is expressed in red color. On the contrary, in Deperm-ME, it can be confirmed that internal magnetization remains very small. Therefore, it was confirmed that Deperm-ME is better than Anhysteretic.

In order to verify the theoretical and simulated results, laboratory-scale experiments using a MTF were performed. A hollow cylinder specimen composed of the SPCC was used as the equivalent model. The specimen and the deperming coil are shown in Fig. 9(a). The length of the specimen is 298 mm, the diameter is 44 mm, and the thickness is 1 mm. To apply the protocol, a solenoid coil of length 60.4 mm and 606 windings was designed.

Figure 9(b) shows the demagnetization system. The specimen was placed inside the coil, and the protocol was applied to the coil using a power supply. The magnetic flux density was measured using a magnetic sensor positioned 18 cm vertically during and after the deperming process. All the devices around the flux sensor were made of nonmagnetic aluminum to minimize the effects of external magnetic fields. In addition, the magnetic field inside the laboratory was set up in a zero magnetic field using a three-axis coil to eliminate the influence of the external magnetic field during the deperming experiment.

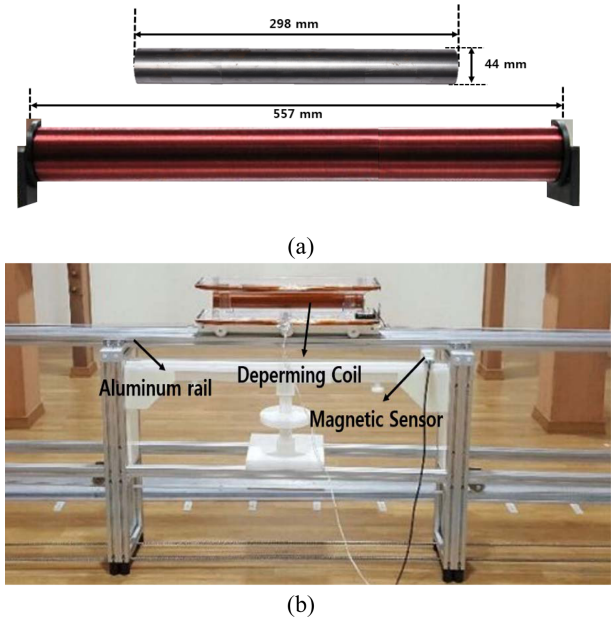

Fig. 9. (Color online) Setup for demagnetization system: (a) Specimen and x-coil. (b) Sensing system.

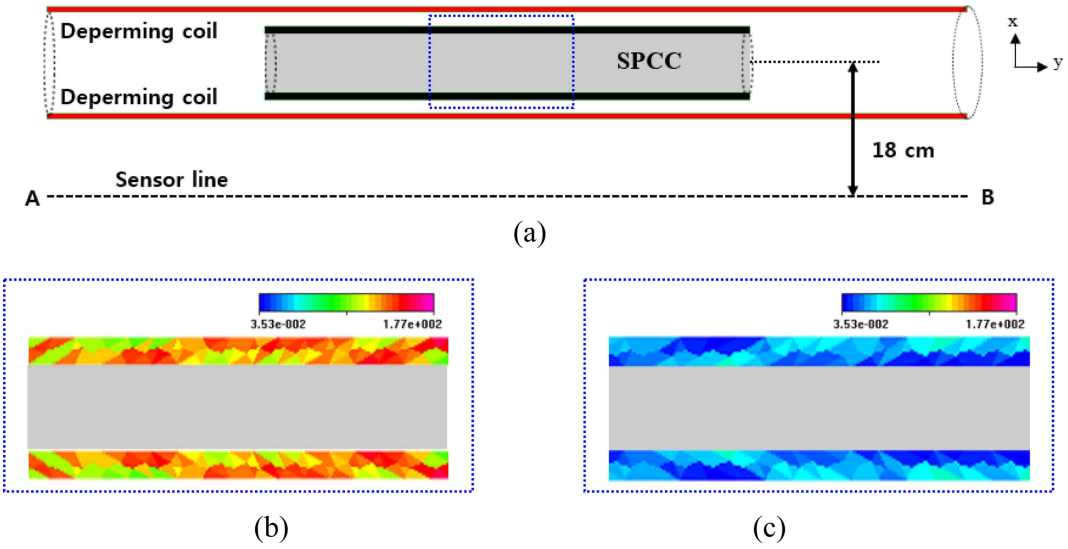

Fig. 8. (Color online) Simulation results according to two protocols: (a) Modeling for simulation. (b) Magnetization distribution in the section after Anhysteretic deperming. (c) Magnetization distribution in the section after Deperm-ME deperming.

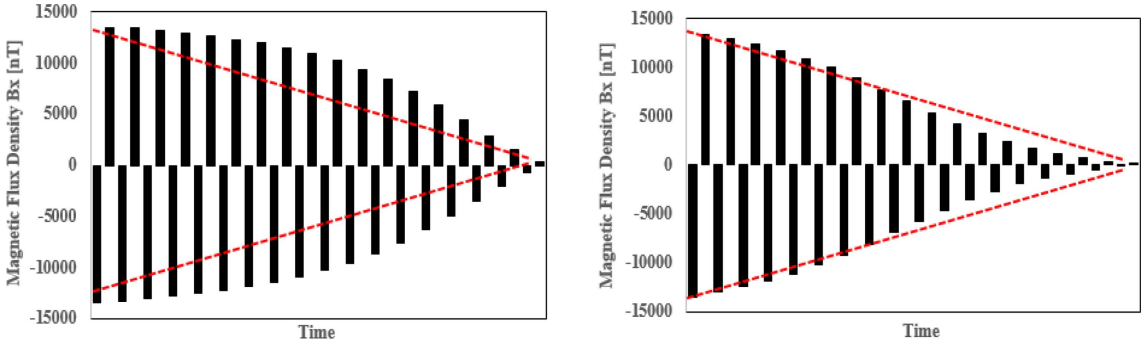

Fig. 10. (Color online) Measured magnetic flux density while applying deperming protocols: (a) Anhysteretic protocol. (b) Deperm-ME protocol.

Table 2. Experimental and simulated results of the specimen.

Deperming protocol	Experiment results		Simulated results	
	Bx [nT]	Bz [nT]	Bx [nT]	Bz [nT]
Anhysteretic	303 nT	292 nT	333.5 nT	310.5
Deperm-ME	40 nT	50 nT	48 nT	55.3 nT

First, the magnetic field inside the specimen was analyzed. Because it is difficult to measure the field, the magnetic flux density was measured using the sensor while each protocol was applied; the results are shown in Fig. 10. In Anhysteretic, the magnetic field is generated in a bell-shaped form, and it was more linear in Deperm-ME. In other words, it is consistent with the theoretical analysis.

After demagnetization, the magnetic field density were measured through a sensor located 18 cm below while the specimen moved along the rail. The longitudinal magnetic field of the specimen is represented by the x component, and the vertical field is represented by the z component. Table 2 compares the maximum magnitude of the magnetic fields measured in the simulation and experiment. For the x component, the largest was measured when the specimen was positioned directly above the sensor, and 303 nT was measured after applying Anhysteretic. However, 40 nT with 87% reduction was measured after applying Deperm-ME. Additionally, the z component was measured largely under both ends of the specimen, it was also reduced by 83%. Further, the results of the analysis and experiment agree with each other.

3.2. Application in scaled warship of SS400 material

The performance of two protocols was verified for a scaled-down warship. It is made of the SS400 material with a length of 1.70 m, a diameter of 0.26 m, and a thickness of 1.6 mm, as shown in Fig. 11(a). Fig. 11(b)

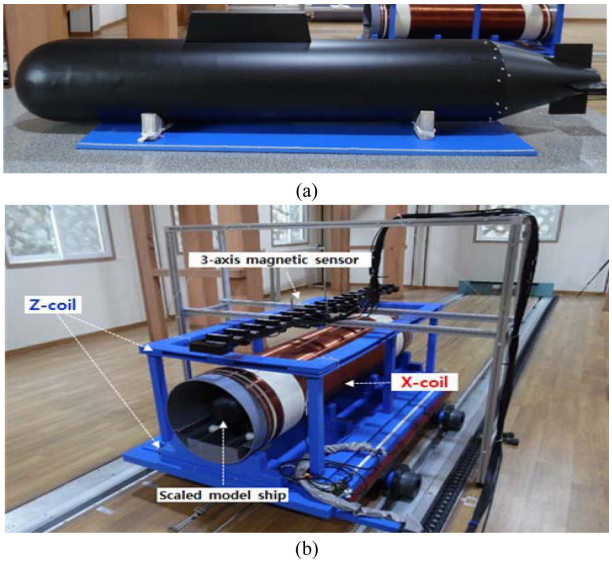

Fig. 11. (Color online) Demagnetization system for a scaled-down warship: (a) The model. (b) X-coil and sensing system.

shows the demagnetization system for the scaled-down warship. To apply the protocol, a solenoid coil of length 2.0 m, a diameter of 0.5 m and 900 windings was designed. In the demagnetization process, the warship was placed inside the coil and the protocol was applied. The protocols in Table 1, which were the same as applied to the specimen, were applied. In order to analyze the effect of the internal magnetic field, the magnetic flux density was measured in a three-axis sensor (Bartington Instruments, Mag 690) positioned 0.29 m above, while applying the protocols. Also, the residual magnetic flux density of the warship was measured after demagnetization, and the results were compared. In addition, all experiments were carried out in a magnetic treatment facility where the earth's magnetic fields was canceled to remove the effect of the external magnetic field.

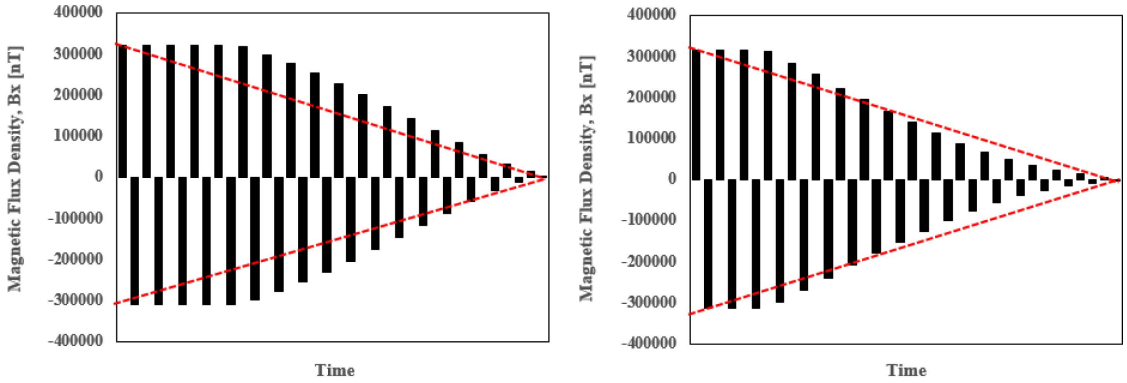

Fig. 12. (Color online) Measured magnetic flux density while applying deperming protocols: (a) Anhysteretic protocol. (b) Deperm-ME protocol.

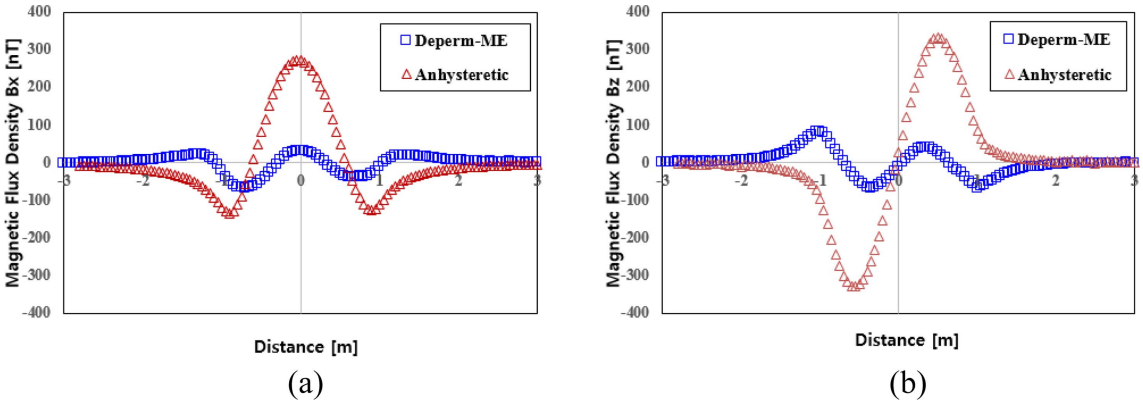

Fig. 13. (Color online) Measured results of demagnetization at the sensor: (a) x-component of magnetic flux density. (b) z-component of magnetic flux density.

Table 3. Measured results of the scaled down warship.

Deperming protocol	Magnetic Flux Density, Bx [nT]	Magnetic Flux Density, Bz [nT]
Anhysteretic	272 nT	332 nT
Deperm-ME	32 nT	83 nT

Figure 12 shows the results measured by the sensor while the two protocols were applied. Regarding the specimen, the decrement became larger in Anhysteretic, and constant in Deperm-ME.

Figure 13 compares the magnetic flux density measured by the sensor after applying the two protocols. Table 3 shows the maximum magnetic flux density. In the Anhysteretic case, 272 nT was measured; however, in the Deperm-ME, 32 nT with 88% reduction was measured. The z component was also reduced by 75%.

4. Conclusion

In this paper, the effect of the demagnetizing field during the deperming process was analyzed by simulations using the combination of the Preisach model and FEM. Further, the effect was proven through experiments on the specimen and a scaled-down warship in a magnetic treatment facility. Owing to the hysteresis characteristics, the demagnetizing field has a nonlinear shape according to the protocols; thus, the magnetic field actually applied inside the warship was changed. Consequently, the variation in Anhysteretic became larger while that in the Deperm-ME has constant variation, thereby diving the Preisach density distribution evenly. Therefore, magnetization was effectively reduced in deperm-ME.

Acknowledgments

This work was supported by the Agency for Defense

Development (No. UD150009DD).

References

[1] M. Enokizono, T. Todaka, and M. Kumoi, J. Magn. Magn. Mater. **112**, 207 (1992).
[2] H. M. J. Boots and K. M. Schep, IEEE Trans. Magn. **36**, 3900 (2000).
[3] G. S. Park, S. Y. Hahn, K. S. Lee, and H. K. Jung, IEEE Trans. Magn. **29**, 1542 (1993).
[4] H. S. Ju, H. J. Chung, S. H. Im, D. W. Jeong, J. W. Kim, H. B. Lee, and G. S. Park, IEEE Trans. Magn. **51**, 7301704 (2015).
[5] T. M. Baynes, G. J. Russel, and A. Bailey, IEEE Trans. Magn. **38**, 1753 (2002).
[6] H. Won, H. S. Ju, S. K. Park, and G. S. Park, IEEE Trans. Magn. **49**, 2045 (2013).
[7] J. W. Kim, S. H. Kim, J. H. Kim, H. J. Chung, and H. B. Lee, J. Magn. **22**, 85 (2017).
[8] Y. H. Kim, K. C. Kim, K. H. Shin, K. S. Yoon, and C. S. Yang, J. Magn. **16**, 453 (2011).
[9] H. S. Ju, H. Won, H. J. Chung, and G. W. Park, J. Magn. **19**, 43 (2014).
[10] J. H. Parq, J. Magn. **22**, 550 (2017).
[11] N. Soda, T. Horri, and M. Kobayashi, IEEE Trans. Magn. **45**, 5289 (2009).
[12] B. K. Pugh, D. P. Kramer, and C. H. Chen, IEEE Trans. Magn. **47**, 4100 (2011).